

EXTRACTION OF MAIN AND SECONDARY ROADS IN VHR IMAGES USING A HIGHER-ORDER PHASE FIELD MODEL

Ting Peng^{a,b}, Ian H. Jermyn^b, Véronique Prinnet^a, Josiane Zerubia^b

^a LIAMA & NLPR, Institute of Automation, Chinese Academy of Sciences, Beijing 100190, China –
(tpeng, prinnet)@nlpr.ia.ac.cn

^b Project-Team Ariana, INRIA/I3S, 06902 Sophia Antipolis, France – (tpeng, ijermyn, jzerubia)@sophia.inria.fr

KEY WORDS: Road, Urban, Satellite, Segmentation, Modelling, Variational methods

ABSTRACT:

This paper addresses the issue of extracting main and secondary road networks in dense urban areas from very high resolution (VHR, ~0.61m) satellite images. The difficulty with secondary roads lies in the low discriminative power of the grey-level distributions of road regions and the background, and the greater effect of occlusions and other noise on narrower roads. To tackle this problem, we use a previously developed higher-order active contour (HOAC) phase field model and augment it with an additional *non-linear* non-local term. The additional term allows separate control of road width and road curvature; thus more precise prior knowledge can be incorporated, and better road prolongation can be achieved for the same width. Promising results on QuickBird panchromatic images at reduced resolutions and comparisons with other models demonstrate the role and the efficiency of our new model.

1. INTRODUCTION

Road extraction from remotely sensed imagery has been extensively studied for the last few decades due to the variety and importance of the potential applications of an automatic extraction method. While a great number of approaches exist in the literature (Fortier et al., 1999, Mena, 2003), the development of reliable procedures is still a challenge. The relative failure of existing approaches stems from the complexity of the imaged scene, *i.e.* the variety of 'objects' (cars, buildings, shadows...) that it contains. Existing algorithms can be classified into three main categories, according to strategy: bottom-up, top-down, and combined. A bottom-up strategy assumes that first basic features are detected, and then constraints are progressively added, up to higher-level recognition. This category includes mathematical morphology (Zhang et al., 1999), knowledge representation and reasoning (Wang and Newkirk, 1988), and road tracking (Geman and Jedynak, 1996, Merlet and Zerubia, 1996). Due to their high sensitivity to nuisance factors, bottom-up methods show strong limitations, and in general, low robustness. A top-down strategy models the objects, and then searches for them in the image. Examples include active contours (Fortier et al., 2001, Mayer et al., 1998) and marked point processes (Stoica et al., 2004, Lacoste et al., 2005). These methods are relatively less sensitive to incomplete and ambiguous information, but the computations needed are usually expensive. In fact, the borderline between the two strategies is not clear. Most methods make use of both bottom-up and top-down processing. In addition, there are also "transversal" techniques, for instance, multi-scale analysis (Mayer et al., 1998), neural networks (Bhattacharya and Parui, 1997), Kalman filters (Vosselman and de Knecht, 1995), and so on.

The algorithms mentioned above are mostly restricted to low-resolution images, and particularly to rural and semi-urban areas, where the road network is readily visible, with little shadow and few occlusion artefacts compared to inner cities. For very high resolution (VHR) imagery in dense urban areas, the complexity of the imaged scenes, which contain many road-like features in the background, undesired noise on the road,

and occlusions caused by trees and the shadows of high buildings (see Figure 1), often results in unreliable road extraction. This is particularly true for secondary roads. Being narrower, they are more affected by the various types of geometric noise present in the image; they are more easily completely occluded, for example. This suggests that more sophisticated road modelling approaches must be developed in order to extract these types of roads in an urban context.



Figure 1. A QuickBird panchromatic image (size = 1400×1400, 0.61m/pixel) of a dense urban area.

In this paper, our goal is to extract the main and secondary road networks in dense urban areas from VHR QuickBird panchromatic images. To do so, we introduce a novel *non-linear* non-local higher-order active contour (HOAC) phase field energy, based on the energy used for the extraction of main road networks in (Peng et al., 2007a). The new, non-linear term allows the long-range interactions between pairs of boundary points on opposite sides of a road to have a different magnitude and/or range from those between pairs of boundary points on the same side of a road. In practical terms, this allows separate control of road width and road curvature: the scale on which the road is modelled as being 'straight' can be different (usually it is larger) from the road width, unlike the model in (Peng et al., 2007a). The effect of this more precise prior

knowledge is better road prolongation and thus better extraction of those roads for which this prior knowledge is crucial, *i.e.* narrower roads. Promising results on QuickBird panchromatic images at reduced resolutions and comparisons with other models demonstrate the role and the efficacy of our new model.

The paper is organised as follows. In section 2, we recall briefly the main principles of the HOAC phase field model of (Peng et al., 2007a), dedicated to the extraction of main road networks. Section 3 introduces the new, non-linear term that differentiates between interactions along the road and across the road, and thus enables more sophisticated prior knowledge to be included. We explain the optimization scheme in section 4. In section 5, the benefits of the new model are illustrated via experiments on real QuickBird panchromatic images. Section 6 concludes.

2. HOAC MODEL FOR MAIN ROAD EXTRACTION

In (Rochery et al., 2006), HOACs were proposed for road network extraction from low to medium resolution images. In contrast to conventional active contours, HOACs incorporate long-range interactions between points on the contour (better called the 'region boundary'), and thus encode complex prior knowledge of road network geometry. For this reason, HOACs are more robust, and can be initialized generically and hence automatically. In (Rochery et al., 2005), 'phase fields' were introduced for region modelling in image processing, and HOACs were reformulated as (non-local) phase field models. We use the phase field framework in this paper, because it has several advantages over parametric active contours or standard level set methods: a linear representation space; ease of implementation; a neutral initialization; and greater topological freedom. To adapt the original phase field HOAC model of (Rochery et al., 2005) to the extraction of the main road network from VHR QuickBird panchromatic images, (Peng et al., 2007b) first proposed a multi-resolution data energy to deal with the complexity of VHR images. For the purpose of further eliminating false detections in the background, (Peng et al., 2007a) introduced *specific* prior knowledge in the form of an outdated GIS map, to complement the *generic* prior knowledge carried by the HOAC prior. It has been experimentally demonstrated that for the main roads, at full resolution, this model is able to keep the unchanged roads, to correct the mistakes, and to extract new roads. However, it is still not capable of retrieving the narrower roads very accurately. In this section, we will briefly review the basic model in (Rochery et al., 2005).

We wish to find the region R in the image domain containing the road network. The phase field framework represents a region by a function $\phi : \Omega \rightarrow \mathfrak{R}$, where $\Omega \subset \mathfrak{R}^2$ is the image domain. The function ϕ defines a region via a threshold $\zeta : R = \{x \in \Omega : \phi(x) > \zeta\}$. To model regions, we define a functional of ϕ ,

$$E_M(\phi; I) = \theta E_p(\phi) + E_D(I, \phi), \quad (1)$$

where $I : \Omega \rightarrow \mathfrak{R}$ is the image data, and θ balances the contributions of the prior energy E_p , which models the

geometry of the region sought, *i.e.* in our case, the region containing the road network, and the data energy E_D , which models the image to be expected given the region. Minimization of such a functional with respect to ϕ gives a

minimizing function ϕ^* , and hence a region R^* . The functional must be designed so that R^* is the region sought.

The prior term E_p in (Rochery et al., 2005) is the sum of two terms: a local phase field term $E_{p,0}$, and a non-local HOAC phase field term $E_{p,NL}$:

$$E_{p,0}(\phi) = \int_{\Omega} dx \left\{ \frac{1}{2} \nabla \phi(x) \cdot \nabla \phi(x) + W(\phi(x)) \right\}, \quad (2a)$$

$$E_{p,NL}(\phi) = -\frac{\beta}{2} \iint_{\Omega^2} dx dx' \nabla \phi(x) \cdot \nabla \phi(x') \Psi\left(\frac{|x-x'|}{d}\right), \quad (2b)$$

where d controls the range of the interaction. The potential function W is

$$W(z) = \lambda \left(\frac{1}{4} z^4 - \frac{1}{2} z^2 \right) + \alpha \left(z - \frac{1}{3} z^3 \right), \quad (3)$$

where λ and α are constants. The potential W effectively constrains $\phi(x) \approx 1$ for $x \in R$ and $\phi(x) \approx -1$ for $x \in \bar{R} = \Omega \setminus R$. As a result, the quantities $\phi_{\pm} = (1 \pm \phi) / 2$ are approximately equal to the characteristic functions of R and \bar{R} . The local gradient product $\nabla \phi(x) \cdot \nabla \phi(x)$ smoothes this result.

Hence, it produces a narrow interface R_C , which is centred around the region boundary ∂R . The interaction function Ψ is

$$\Psi(r) = \begin{cases} \frac{1}{2} (2 - |r| + \frac{1}{\pi} \sin(\pi |r|)) & \text{if } |r| < 2, \\ 0 & \text{else.} \end{cases} \quad (4)$$

The energy $E_{p,0}$ is equivalent to an active contour model whose energy is a linear combination of region boundary length and region area. $E_{p,NL}$ describes long-range interactions between the gradient vectors of ϕ at pairs of points. Since $\nabla \phi$ is only non-zero in R_C , this is the same as long-range interactions between pairs of region boundary points and their normal vectors. Its effect is to prevent pairs of boundary points with antiparallel normal vectors from coming too close, and to encourage the growth of arm-like shapes. Therefore, E_p favours regions

composed of long, low curvature 'arms' of roughly constant width that meet at junctions, *i.e.* it models network structures.

ads from the back-ground. We model the one point statistics of the image intensities, *i.e.* their histograms. It consists of two parts: information from the roads and from the background. E_D can be written as

$$E_D(I, \phi) = - \int_{\Omega} dx \{ \ln P_+(I(x))\phi_+(x) + \ln P_-(I(x))\phi_-(x) \} .(5)$$

P_{\pm} are two-component Gaussian mixture distributions, modeling the image intensities, where $+$ denotes the roads and $-$ denotes the background. Their parameters are learned on samples of road and non-road in the image by supervised learning.

3. NON-LINEAR TERM FOR SECONDARY ROAD EXTRACTION

Compared to the main roads, the secondary roads are much more difficult to deal with, for the following reasons. First, the radiometric properties of narrower roads are similar to those of the background. Second, narrower roads are more often obscured by shadows and trees, which can cause gaps in the extracted network. For both reasons, data driven/bottom-up models fail to retrieve the roads correctly: strong geometric prior information is needed. The network model of equation (2b) contains such prior knowledge, but it suffers from a limitation that is severe in the case of secondary roads: the interaction between points on opposite sides of a road ($\nabla\phi(x) \cdot \nabla\phi(x') < 0$) is of the same strength and range as the interaction between points on the same side of a road ($\nabla\phi(x) \cdot \nabla\phi(x') > 0$). This means that the scale on which the road is expected to be straight is the same as the width of the road, whereas in fact road width gives only an (approximate) upper bound on the radius of curvature of the road: most roads are straighter than they are wide. For narrow roads this is particularly problematic, since the road region is relatively unconstrained due to the small road width. In particular, road prolongation is short-range just when, due to the effects of geometric noise mentioned above, we want it to be long-range.

In order to change this situation, we need to be able to model longer-range, stronger interactions along the road without changing the interactions across the road, *i.e.* we have to separate the two interactions. In this section, we will achieve this goal by introducing a new energy term. To motivate this term, we return to the contour formulation.

3.1 Interaction functions

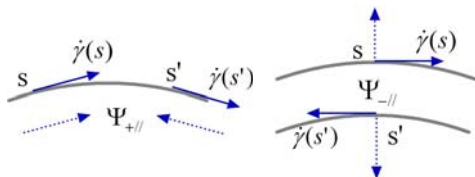


Figure 2. The interactions $\Psi_{+//}$ and $\Psi_{-//}$

The data term E_D takes into account the radiometric properties of dense urban areas, which discriminate roads. Since roads are elongated structures, the interaction between points on the same side of a road must have longer range (or be stronger, which often amounts to nearly the same thing) than the interaction between points on opposite sides of a road. To achieve this goal, a straightforward solution is to separate the interaction function along one side of a road $\Psi_{+//}$ from the one across a road $\Psi_{-//}$, as shown in Figure 2. In other words, the interaction function must depend on the tangent/normal vectors at the pairs of points that are its argument. Although the length scale in the interaction function, d , could be made to depend on the inner product between the tangent/normal vectors at the two pixels, it would lead to complicated functional derivatives. Alternatively, we prefer to perform a linear interpolation between two interaction functions. In the contour formulation, our new HOAC prior energy $E_{P,HO}$ takes the form:

$$E_{P,HO}(\gamma) = - \iint_{s' \times s} ds ds' \{ f_{+//}(\dot{\gamma}(s) \cdot \dot{\gamma}(s')) \Psi_{+//} - f_{-//}(\dot{\gamma}(s) \cdot \dot{\gamma}(s')) \Psi_{-//} \} , \quad (6)$$

where $\gamma : S^1 \rightarrow \Omega$, is an arc length parameterization of the region boundary ∂R , instead of the entire image domain; $\dot{\gamma}(s)$ is the tangent vector to the boundary at s (thus $\dot{\gamma}(s) \cdot \dot{\gamma}(s') \in [-1, 1]$); ' $+//$ ' denotes parallel vectors and ' $-//$ ' denotes antiparallel vectors. $f_{+//}(x), f_{-//}(x) : [-1, 1] \rightarrow [0, 1]$ are two linear functions:

$$f_{+//}(x) = (1+x)/2 , \quad (7a)$$

$$f_{-//}(x) = (1-x)/2 . \quad (7b)$$

$\Psi_{+//}$ and $\Psi_{-//}$ are the same types of function as in equation (4), but have different range or magnitude. The two interaction functions compete with each other: when $\dot{\gamma}(s) \cdot \dot{\gamma}(s') \in [0, 1]$, *i.e.* the two interacting tangent vectors are more parallel, $\Psi_{+//}$ is dominant; while when $\dot{\gamma}(s) \cdot \dot{\gamma}(s') \in [-1, 0]$, *i.e.* the two interacting tangent vectors are more antiparallel, $\Psi_{-//}$ is dominant. To simplify the formulation, we adjust only the magnitude of the interaction (although this effectively changes its range also), and we further assume that the magnitude of the interaction of parallel vectors is stronger than that of antiparallel vectors, *i.e.* $\Psi_{+//} = a\Psi_{-//}$, where $a > 1$, is a constant. Equation (6) becomes

$$E_{p,HO}(\gamma) = -\frac{1}{2} \iint_{s \times s'} ds ds' \{ [(a-1) + (a+1)\dot{\gamma}(s) \cdot \dot{\gamma}(s')] \Psi_{-l} \} \quad (8)$$

3.2 Non-linear non-local HOAC phase field energy

In order to implement $E_{p,HO}(\gamma)$ in the phase field framework, it needs to be reformulated as a function of the phase field ϕ , instead of the arc length parameterization γ used in equation (8). To this end, we replace tangent vectors by normal vectors, and then normal vectors by $\nabla\phi$. Subsequently, the range of interactions is extended from the region boundary ∂R to the whole of the image domain Ω . Due to the fact that $\nabla\phi(x)$ is approximately equal to zero everywhere outside the narrow interface R_C in Ω , the boundary indicator function

$$S(\phi) = (\nabla\phi(x) \cdot \nabla\phi(x'))(\nabla\phi(x') \cdot \nabla\phi(x')) \quad (9)$$

is inserted into the first term of equation (8). Thus we have

$$E_{p,HO}(\phi) = -\frac{1}{2} \iint_{\Omega^2} dx dx' \{ [(a-1)S(\phi) + (a+1)\nabla\phi(x) \cdot \nabla\phi(x')] \Psi\left(\frac{|x-x'|}{d}\right) \} \quad (10)$$

When $a = 1$, this reduces to the non-local HOAC phase field term $E_{p,NL}$ of equation (2b) (up to a factor of $\beta/2$). Therefore, we define our new additional energy term by

$$E_{p,NEW}(\phi) = -\frac{\beta_2}{4} \iint_{\Omega^2} dx dx' \{ S(\phi) \Psi\left(\frac{|x-x'|}{d}\right) \} \quad (11)$$

Since the functional derivative of $E_{p,NEW}$ will, unlike that of $E_{p,NL}$, contain a term non-linear in ϕ due to $S(\phi)$ being $O(\phi^4)$, we refer to it as the *non-linear* non-local term. We now define our new model as $E = \theta(E_{p,0} + E_{p,NL} + E_{p,NEW}) + E_D$.

Note that whether the two tangent/normal vectors at a pair of in-teracting points are parallel or antiparallel, the effect of $E_{p,NEW}$ is always to encourage two points inside the range of the interaction to attract each other. Thus $E_{p,NEW}$ reinforces the effect of $E_{p,NL}$ in the case that the tangent/normal vectors are parallel, and it partly annuls the effect of $E_{p,NL}$ in the case that the tangent/normal vectors are antiparallel. Accordingly, the interaction between pairs of points on the same side of a road is

stronger than that between pairs of points on opposite sides of a road.

4. OPTIMIZATION

We now want to find the function ϕ that minimizes our new total energy E . Using gradient descent, at convergence, the optimal ϕ^* determines an estimate of the road network. Following (Rochery et al., 2005), we use a neutral initialization, *i.e.* the initial value of ϕ is set equal to a constant everywhere in Ω . During the iterations, no re-initialization or regularization is required. To perform gradient descent we need only the functional derivative of E :

$$\begin{aligned} \frac{\delta E}{\delta\phi(x)} = & \frac{1}{2} \ln \frac{P}{P_+} + \theta \{-\nabla^2\phi(x) + \lambda(\phi^3(x) - \phi(x)) \\ & + \alpha(1 - \phi^2(x)) + \beta \int_{\Omega} dx' \phi(x') \nabla^2 \Psi\left(\frac{|x-x'|}{d}\right) \\ & + \beta_2 \nabla \cdot [\nabla\phi(x) \int_{\Omega} dx' (\nabla\phi(x') \cdot \nabla\phi(x')) \Psi\left(\frac{|x-x'|}{d}\right)] \} \quad (12) \end{aligned}$$

The derivatives $\delta E_{p,NL} / \delta\phi$ and $\delta E_{p,NEW} / \delta\phi$ are non-local. To avoid performing explicit convolutions, they are calculated in the Fourier domain. The resulting evolution equation is

$$\begin{aligned} \frac{\partial\phi(x)}{\partial t} = & \frac{1}{2} \ln \frac{P}{P_-} + \theta \{\nabla^2\phi(x) - \lambda(\phi^3(x) - \phi(x)) \\ & - \alpha(1 - \phi^2(x)) + \beta F^{-1} \{ k^2 d \hat{\Psi}(kd) \hat{\phi}(k) \} \\ & - \beta_2 \nabla^2\phi(x) F^{-1} \{ d \hat{\Psi}(kd) F \{ \nabla\phi(x) \cdot \nabla\phi(x) \} \} \\ & - \beta_2 \nabla\phi(x) \cdot \nabla \{ F^{-1} \{ d \hat{\Psi}(kd) F \{ \nabla\phi(x) \cdot \nabla\phi(x) \} \} \} \}, \quad (13) \end{aligned}$$

where F and F^{-1} denote the Fourier and the inverse Fourier transform respectively, and $\hat{\cdot}$ indicates the Fourier transform of a variable. In the discretized implementation, all derivatives are computed in the Fourier domain, while the time evolution uses the forward Euler method. The parameters of the prior energy, *i.e.* $\theta, \alpha, \lambda, \beta, \beta_2$, and d are constrained by stability conditions that ensure that a long bar of a given width is a stable configuration of the model. This enables a choice of λ, β, β_2 , and d based on the expected road width: only α and θ remain.

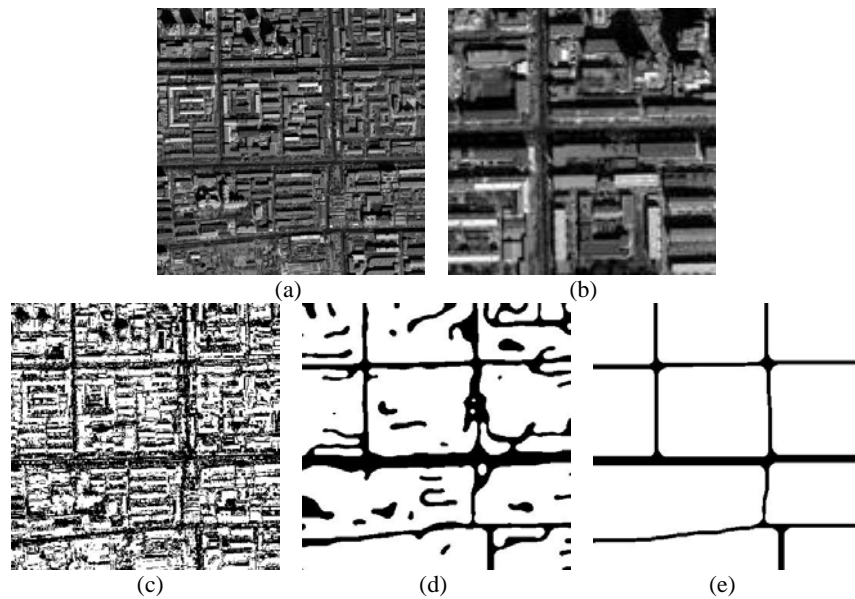


Figure 3. Experiments at 1/4 resolution. 3(a)-3(b): image data (size = 350×350 , road width = 3~5 pixels) and its partial enlargement. 3(c)-3(e): results obtained using the energy E (with $E_{P,NEW}$) at iterations 1, 1,500 and 27,000.

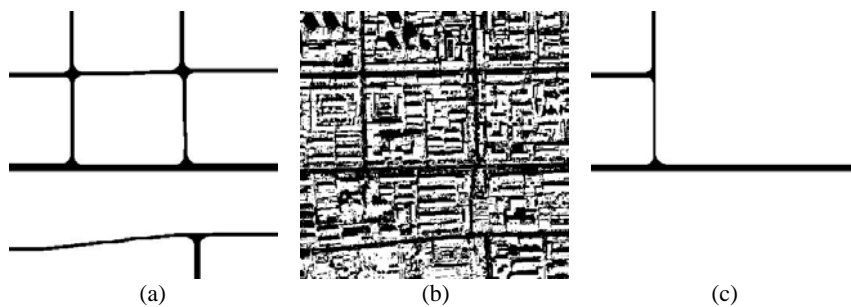


Figure 4. Experiments at 1/4 resolution. Left to right: results obtained respectively using the energy E_M (without $E_{P,NEW}$), maximum likelihood estimation, and a standard, non-higher-order active contour model (with neither $E_{P,NL}$ nor $E_{P,NEW}$).

5. RESULTS AND COMPARISONS

In this section, we demonstrate the behaviour of our new model containing the non-linear, non-local HOAC term $E_{P,NEW}$ via experiments on real QuickBird panchromatic images in dense urban areas, at reduced resolutions.

Figure 3(a) shows one of the input images at 1/4 resolution. Figure 3(b) shows its partial enlargement, to display the complexity remaining at this resolution. The parameters $(\theta, \alpha, \lambda, \beta, \beta_2, d)$ were $(100, 0.12, 3.8, 0.0375, 0.0338, 4)$. The results obtained using the energy with the new non-linear non-local term $E_{P,NEW}$ at iterations 1, 1,500 and 27,000 are illustrated in Figures 3(c)-3(e). The result obtained using the energy E_M (without $E_{P,NEW}$) is shown in Figure 4(a). We see that adding $E_{P,NEW}$ enables the recovery of the main and secondary road network, whereas the model without $E_{P,NEW}$ misses a secondary

road. In order to illustrate the effects of other terms in the model, we computed results using maximum likelihood estimation (*i.e.* $\theta = 0$) and a standard, non-higher-order active contour, *i.e.* $\beta = \beta_2 = 0$ (see Figures 4(b) and 4(c)). The MLE result shows that local image information alone is not sufficient to distinguish the roads from the background, while the standard active contour result shows the importance of the geometric knowledge introduced by HOACs. Quantitative evaluations based on standard criteria (Heipke et al., 1997) are shown in Table 1. Ground truth for the evaluations was segmented by hand. On the other hand, the computation time for the result in Figure 3 was around 80 minutes, which is considerably slower than the next nearest time, that obtained with the model E_M (Figure 4(a)). Figure 5 presents more results at reduced resolutions. The first column shows the input image data, which is either at 1/4 or 1/2 resolution. The two columns on the right show the corresponding results obtained with and without the new non-linear, non-local term $E_{P,NEW}$.

The importance of $E_{P,NEW}$ is clear: it facilitates greatly the retrieval of secondary roads.

Image	Completeness TP/(TP+FN)	Correctness TP/(TP+FP)	Quality TP/(TP+FP+F N)
New model E (Figure 3(e))	0.9989	0.9312	0.9303
E_M ($\beta_2 = 0$) (Figure 4(a))	0.9575	0.9334	0.8963
$\theta E_{P,0} + E_D$ (Figure 4(c))	0.4895	0.9208	0.4698
MLE ($\theta = 0$) (Figure 4(b))	0.9928	0.2115	0.2112

Table 1. Quantitative evaluation criteria of the different methods (T = True, F = False, P = Positive, N = Negative)

6. CONCLUSIONS

Narrow secondary roads in VHR images are very difficult to extract, because of occlusion effects and the similar radiometric

properties of the road region and background. To tackle this problem, the incorporation of strong geometric prior knowledge of road networks is essential. Building upon previous work dedicated to segmenting only main road networks, we have presented, in this paper, a novel *non-linear*, non-local phase field term, and applied it to the extraction of main and secondary road networks in VHR images. This novel term causes pairs of points inside the range of the interaction to attract each other. In conjunction with the original HOAC geometric term, it allows the interaction between points on the same side of a road to be stronger than the interaction between points on opposite sides of a road. Therefore, the incorporation of the term enables the generation of longer arm-like branches and better prolongation. Experiments on road network extraction from QuickBird panchromatic images in dense urban areas at reduced resolution show that road networks are completely recovered using the model with the additional term. The new model clearly outperforms the previous model in terms of quality of results. However, the new model is computationally expensive, which is why the method was applied at reduced resolution. To solve this problem, which is due to the non-linear nature of the new term, we are now working on a novel *linear* non-local prior term that will have a similar effect.

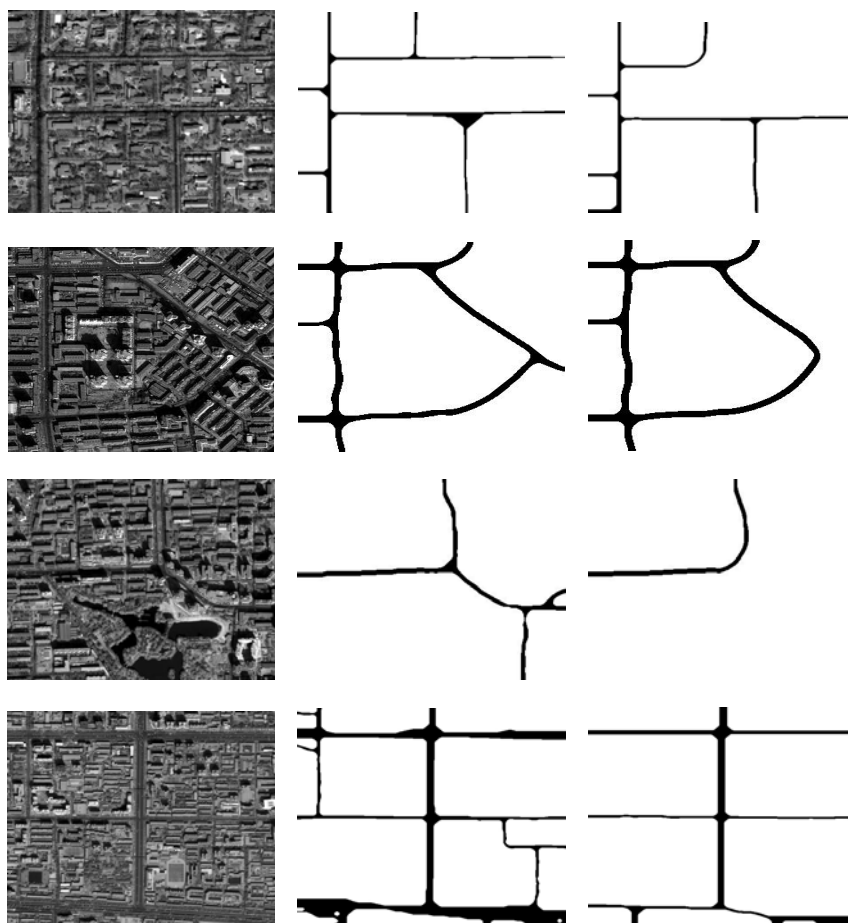


Figure 5. More experiments at reduced resolutions. First column: input images, first row: 1/2 resolution, size = 440×400 , road width = 2~4 pixels; second row: 1/4 resolution, size = 300×300 , road width = 3~5 pixels; third row: 1/4 resolution, size = 400×300 , road width = 3~6 pixels; last row: 1/4 resolution, size = 512×512 , road width = 3~15 pixels. Two rightmost columns: corresponding results obtained using the energy E (with $E_{P,NEW}$) and the energy E_M (without $E_{P,NEW}$).

ACKNOWLEDGEMENTS

This work was partially supported by European Union Network of Excellence MUSCLE (FP6-507752). The work of the first author is supported by an MAE/Thales Alenia Space/LIAMA grant.

REFERENCES

- Bhattacharya, U. and Parui, S., 1997. An improved backpropagation neural network for detection of road-like features in satellite imagery. *International Journal of Remote Sensing* 18(16), pp. 3379–3394.
- Fortier, M. F. A., Ziou, D., Armenakis, C. and Wang, S., 1999. Survey of work on road extraction in aerial and satellite images. Technical Report 241, Université de Sherbrooke, Quebec, Canada.
- Fortier, M. F. A., Ziou, D., Armenakis, C. and Wang, S., 2001. Automated correction and updating of road databases from high-resolution imagery. *Canadian Journal of Remote Sensing* 27(1), pp. 76–89.
- Geman, D. and Jedynak, B., 1996. An active testing model for tracking roads in satellite images. *IEEE Trans. Pattern Analysis and Machine Intelligence* 18(1), pp. 1–14.
- Heipke, C., Mayr, H., Wiedemann, C. and Jamet, O., 1997. Evaluation of automatic road extraction. *International Archives of Photogrammetry and Remote Sensing XXXII*, pp. 47–56.
- Lacoste, C., Descombes, X. and Zerubia, J., 2005. Point processes for unsupervised line network extraction in remote sensing. *IEEE Trans. Pattern Analysis and Machine Intelligence* 27(10), pp. 1568–1579.
- Mayer, H., Laptev, I. and Baumgartner, A., 1998. Multi-scale and snakes for automatic road extraction. In: *Proc. European Conference on Computer Vision (ECCV)*, Vol. 1, Freiburg, Germany.
- Mena, J., 2003. State of the art on automatic road extraction for GIS update: A novel classification. *Pattern Recognition Letters* 24(16), pp. 3037–3058.
- Merlet, N. and Zerubia, J., 1996. New prospects in line detection by dynamic programming. *IEEE Trans. Pattern Analysis and Machine Intelligence* 18(4), pp. 426–431.
- Peng, T., Jermyn, I. H., Prinnet, V., Zerubia, J. and Hu, B., 2007a. A phase field model incorporating generic and specific prior knowledge applied to road network extraction from VHR satellite images. In: *Proc. British Machine Vision Conference (BMVC)*, Warwick, England.
- Peng, T., Jermyn, I. H., Prinnet, V., Zerubia, J. and Hu, B., 2007b. Urban road extraction from VHR images using a multiscale approach and a phase field model of network geometry. In: *Proc. 4th IEEE GRSS/ISPRS Joint Workshop on Remote Sensing and Data Fusion over Urban Areas (URBAN)*, Paris, France.
- Rochery, M., Jermyn, I. H. and Zerubia, J., 2005. Phase field models and higher-order active contours. In: *Proc. IEEE International Conference on Computer Vision (ICCV)*, Beijing, China.
- Rochery, M., Jermyn, I. H. and Zerubia, J., 2006. Higher-order active contours. *International Journal of Computer Vision* 69(1), pp. 27–42.
- Stoica, R., Descombes, X. and Zerubia, J., 2004. A Gibbs point process for road extraction from remotely sensed images. *International Journal of Computer Vision* 57(2), pp. 121–136.
- Vosselman, G. and de Knecht, J., 1995. Road tracing by profile matching and Kalman filtering. In: *Proc. Workshop on Automatic Extraction of Man-Made Objects from Aerial and Space Images*, Birkhuser Verlag, Basel-Boston-Berlin.
- Wang, F. and Newkirk, R., 1988. A knowledge-based system for highway network extraction. *IEEE Trans. Geoscience and Remote Sensing* 26, pp. 525–531.
- Zhang, C., Murai, S. and Baltsavias, E. P., 1999. Road network detection by mathematical morphology. In: *Proc. of ISPRS Workshop '3D Geospatial Data Production: Meeting Application Requirements'*, Paris, France.

